Atmos. Meas. Tech., 8, 5289–5299, 2015
www.atmos-meas-tech.net/8/5289/2015/
doi:10.5194/amt-8-5289-2015

Atmospheric Measurement Techniques
Open Access
EGU

Gas adsorption and desorption effects on cylinders and their importance for long-term gas records

M. C. Leuenberger, M. F. Schibig, and P. Nyfeler

Climate and Environmental Physics, Physics Institute and Oeschger Centre for Climate Change Research, University of Bern, Switzerland

Correspondence to: M. C. Leuenberger (leuenberger@climate.unibe.ch)

Received: 11 May 2015 – Published in Atmos. Meas. Tech. Discuss.: 4 August 2015
Revised: 27 November 2015 – Accepted: 27 November 2015 – Published: 18 December 2015

Abstract. It is well known that gases adsorb on many surfaces, in particular metal surfaces. There are two main forms responsible for these effects (i) physisorption and (ii) chemisorption. Physisorption is associated with lower binding energies in the order of 1–10 kJ mol^{-1}, compared to chemisorption which ranges from 100 to 1000 kJ mol^{-1}. Furthermore, chemisorption only forms monolayers, contrasting physisorption that can form multilayer adsorption. The reverse process is called desorption and follows similar mathematical laws; however, it can be influenced by hysteresis effects. In the present experiment, we investigated the adsorption/desorption phenomena on three steel and three aluminium cylinders containing compressed air in our laboratory and under controlled conditions in a climate chamber, respectively. Our observations from completely decanting one steel and two aluminium cylinders are in agreement with the pressure dependence of physisorption for CO_2, CH_4, and H_2O. The CO_2 results for both cylinder types are in excellent agreement with the pressure dependence of a monolayer adsorption model. However, mole fraction changes due to adsorption on aluminium (< 0.05 and 0 ppm for CO_2 and H_2O) were significantly lower than on steel (< 0.41 ppm and about < 2.5 ppm, respectively). The CO_2 amount adsorbed (5.8×10^{19} CO_2 molecules) corresponds to about the fivefold monolayer adsorption, indicating that the effective surface exposed for adsorption is significantly larger than the geometric surface area. Adsorption/desorption effects were minimal for CH_4 and for CO but require further attention since they were only studied on one aluminium cylinder with a very low mole fraction. In the climate chamber, the cylinders were exposed to temperatures between −10 and +50 °C to determine the corresponding temperature coefficients of adsorption. Again, we found distinctly different values for CO_2, ranging from 0.0014 to 0.0184 ppm °C^{-1} for steel cylinders and −0.0002 to −0.0003 ppm °C^{-1} for aluminium cylinders. The reversed temperature dependence for aluminium cylinders points to significantly lower desorption energies than for steel cylinders and due to the small values, they might at least partly be influenced by temperature, permeation from/to sealing materials, and gas-consumption-induced pressure changes. Temperature coefficients for CH_4, CO, and H_2O adsorption were, within their error bands, insignificant. These results do indicate the need for careful selection and usage of gas cylinders for high-precision calibration purposes such as requested in trace gas applications.

1 Introduction

Precision and accuracy of trace gas mole fractions of ambient air composition depend among other factors on the stability of primary and secondary standards. Several studies in the past have documented instabilities of gas composition in high-pressure cylinders. These instabilities can either be viewed as temporal drifts of gas composition or as pressure-dependent composition changes along the lifetime of the cylinder gas. These drifts have been attributed to numerous diffusional fractionation processes such as ordinary diffusion (depending on molecular mass and molecular size), thermal diffusion, or effusion (Bender et al., 1994; Keeling et al., 1998, 2007; Langenfelds et al., 2005), or were related to surface interaction alterations (Yokohata et al., 1985). These latter processes, i.e. adsorption and desorption, have been investigated in more detail and play an important role regarding

gas composition stability, in particular for trace gas species. Besides the choice of the metal, surface condition, surface coating or finish, as well as the humidity, are also critical for the gas composition (Matsumoto et al., 2005). The presented work was motivated by the fact that adsorption/desorption effects have been observed to play an important role not only in the laboratory, but also in the field during different experimental setups (Berhanu et al., 2015; Schibig et al., 2015).

In sorption theory, one distinguishes several terms such as absorption, adsorption, sorption, desorption, physisorption, and chemisorption. Adsorption is a surface adhesion process of atoms, ions, or molecules from a gas, liquid, or dissolved solid (adsorbate), resulting in a layer on the adsorbent surface (main material). In contrast, absorption is a volume process in which permeation or dissolution of the absorbate in a liquid or solid material (absorbent) takes place. Sorption summarizes both processes, while desorption is the reverse process.

Surface atoms of the bulk material, specified by the fact that they are not fully surrounded by other adsorbent atoms, can therefore attract adsorbates. Adsorption itself splits into physisorption and chemisorption. The former is a general phenomenon forming mono- or multilayers, whereas the latter depends on the chemical feature of both the adsorbate and adsorbent, and forms only monolayers. Similar to surface tension, adsorption is a consequence of surface energy.

Physical adsorption, also known as physisorption, is a process governed by low electrostatic interactions between the electron configuration of the adsorbate and the adsorbent, in particular van der Waals forces. The involved energy is weak (10–100 meV corresponding to 1–10 kJ mol^{-1}) and therefore barely influences the electron structure of the substances involved, and it mainly appears under low temperature conditions (room energy). The upper energy limit involves the interaction with permanent electric dipoles of polar surfaces (salts) or with the image charges as present in electrically conductible surfaces such as metals. For these processes the energies can reach those of chemisorption.

Chemisorption in contrast involves much higher energies in the range of 1 to 10 eV (100 to 1000 kJ mol^{-1}) and often requires an activation energy, finally resulting in a structure that is similar to a chemical bond of either ionic or covalent type. Sorption and desorption can differ; in this case we deal with hysteresis; i.e. the quantity adsorbed differs from the corresponding quantity desorbed.

Several mathematical models have been presented for adsorption. Equation (1) expresses the pressure dependence by adjusting the empirical constants k and n. x denotes the quantity adsorbed, m the mass of absorbent, and P the pressure (Freundlich, 1906).

$$\frac{x}{m} = kP^{1/n} \tag{1}$$

Irving Langmuir (Langmuir, 1916, 1918) was the first to derive a scientifically based adsorption isotherm. It is based on four assumptions. (i) All of the adsorption sites are equivalent and each site can only accommodate one molecule. (ii) The surface is energetically homogeneous and adsorbed molecules do not interact. (iii) There are no phase transitions. (iv) At the maximum adsorption, only a monolayer is formed. Adsorption only occurs on localized sites on the surface, not with other adsorbates. His final result expresses the fraction of the adsorption sites occupied, Θ, as given in Eq. (2):

$$\Theta = \frac{KP}{1+KP}, \tag{2}$$

where K is the ratio of the direct (adsorption) and reverse rate (desorption) constants (k, k_{-1}), and P is the pressure. For low pressures, Θ corresponds to KP, and for high pressure it approaches unity.

The four assumptions listed by Langmuir are often not fulfilled, in particular, assumption (iv); but an in depth discussion of these issues would exceed the scope of this publication. However, in our experiments we found a good agreement with this simplified adsorption theory. Besides the pressure or gas (particle) density dependence, there is also a temperature dependence of adsorption/desorption processes. According to the Polanyi–Wigner equation given in Eq. (3), the desorption rate (k_{-1}) is dependent on time, t, on a frequency term, $\upsilon(\Theta)$, a coverage-order term, Θ^n, and an Arrhenius factor containing the activation energy, $E = E(\Theta)$, for desorption.

$$k_{-1}(\Theta T(t)) = -\frac{\mathrm{d}\Theta}{\mathrm{d}t} = \upsilon(\Theta)\cdot\Theta^n\cdot e^{-\left(\frac{E(\Theta)}{R\cdot T(t)}\right)} \tag{3}$$

A similar equation can be written for adsorption; however the adsorption energy is significantly lower, such that the equilibrium conditions are characterized by the desorption energy. Following the van't Hoff equation, different equilibrium conditions, $K(T)$ and $K(T_0)$, can be represented by

$$K(T) = \frac{k(T)}{k_{-1}(T)} = K(T_0)\cdot e^{\frac{E}{R}\cdot\left(\frac{1}{T}-\frac{1}{T_0}\right)}. \tag{4}$$

In this work we mainly investigate the adsorption and its reverse process. In particular we present results for the pressure- and temperature-dependent adsorption process of trace gases (CO_2, CO, CH_4) as well as H_2O on two metal surfaces, namely steel and aluminium, using the cylinders tabulated in Table 1.

2 Methods

We ran two experiments in order to determine the pressure and temperature dependencies of gas adsorption on two different metal cylinder surfaces (steel and aluminium). We used 50 L tempered steel (34CrMo4) cylinders equipped with a standard brass valve K44-8 from VTI with PEEK as spindle-sealing material. The regulator connection type is G 5/8″ RH (right-handed) female thread from Carbagas,

Table 1. Cylinders used for the two experiments with their identification and trace gas mole fractions. Note that the absolute values of both CO and H_2O are of lower quality due to values close to the lower end of the measurement range. Note that no pretreatment of cylinders has been applied by us, i.e. no steam cleaning, surface conditioning, or finishing, except that applied by the supplier (see main text). Values displayed in figures are non-calibrated values.

Cylinder	Initial pressure (bar)	Final pressure (bar)	CO_2 (ppm)	CO (ppb)	CH_4 (ppb)	H_2O (ppm)	Calibration laboratory
Experiment 1							
LK542039	106	1	412.26	NA	2095.55	4.5	Bern
CB09790	97	1	406.44	9.5	1976.75	15	Bern
CB09880	58	1	393.42	NA	1938.86	8.9	Bern
Experiment 2							
1: LK502291	153.2	138.7	440.64	10.40	2058.0	0.88	Bern
2: CB09790	121.3	97.2	405.88	5.40	1977.04	2.4	Bern
3: LK548602	155.0	140.5	421.42	9.40	1967.04	0	Bern
4: CB09877	131.0	106.9	400.30	193.40	2080.04	28.4	Empa
5: LK548528	153.6	139.1	440.00	13.40	2058.04	2.9	Bern
5[a] LK535353	> 170[b]	155.5	392.22	74.40	1995.04	17.7	Bern
6: CB09786	120.5	96.4	406.42	11.40	1977.04	4.9	Bern
7: CA03901	76	75	363.62	102.4	1796.04	1.2	NOAA

[a] Due to a leak, cylinder LK548528 had to be exchanged for cylinder LK535353 during the experiment.
[b] The pressure reading was made at 45 °C; the pressure comparable to the other pressure readings taken at 22 °C will be lower.

Switzerland, sealed with a PA (nylon) disk. Gas wetted materials for these cylinders are steel, brass, and PEEK. The aluminium cylinders are new 30 L Scott-Marrin Luxfer (AA 6061 T6) cylinders equipped with a brass valve D 202 from Rotarex with PA as spindle material. The regulator connection type is CGA-590. Gas-wetted materials are aluminium, stainless steel, brass, and PA. No additional pre-treatment of the inner surfaces was applied, except that applied by the supplier and producer that we do not know in detail, as well as that given above. The steel cylinders were filled by Carbogas according to their protocol. We do not know the filling history of these cylinders except that they are used for compressed air fillings only. The aluminium cylinders were pumped three times to roughly 10 mbar and then flushed and pressurized to 10 to 15 bar using dry compressed air with ambient mole fractions, and then filled with dry compressed air from another cylinder again at ambient mole fractions. CB09877 was prepared similarly at Empa and was additionally blended by a second compressed air cylinder. CA03901 was prepared at Boulder by NOAA/CMDL according to their protocol. In the first experiment we decanted 5 L min^{-1} from both steel and aluminium cylinders. The cylinder's mole fractions of CO_2, CH_4, and H_2O were monitored by a Picarro G2311f and G2401, in which case CO was measured in addition. Attached to the vertically standing cylinders were pressure regulators from Tescom (type: 64-3441KA412 dual stage). The starting pressures were about 110 and 95 bar for the steel and aluminium cylinder, respectively. Due to the large gas flow which was maintained by the detector itself in the case of G2311f and by an external flow controller for the G2401, it took only about 14 h (steel) and 8 h (aluminium), respectively, to empty the cylinders. The mole fractions were monitored on a 0.1 s level with the G2311f instrument, whereas they were monitored on a 5 s level with the G2401. In parallel, we recorded the pressure continuously. This experiment was performed at the University of Bern under normal laboratory conditions (room temperature was 22 °C; room pressure was about 950 mbar).

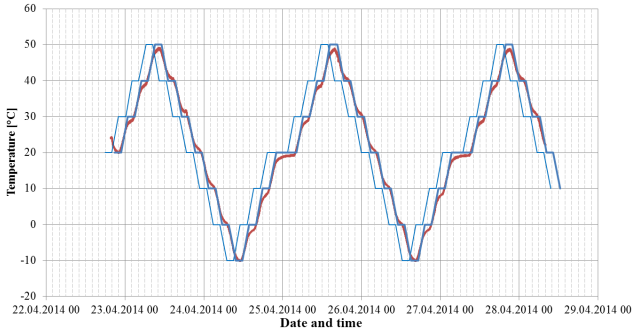

Figure 1. Temperature exposed to the cylinders in the climate chamber. Every 2 h, the temperature changed by 10 °C. The actual temperature (red line) follows the set temperature (light blue) with a delay of 2.75 h (the bold blue line accounts for the time shift).

The second experiment was performed in the climate chamber at the Swiss Federal Institute of Metrology (METAS). The purpose of this experiment was to determine the temperature dependence of the adsorption/desorption process. Gas usage in experiment 2 was designed to be far less than that in experiment 1. Eight cylinders (five steel and three aluminium) were tested over a temperature range from −10 to +50 °C as documented in Fig. 1. The temperature was set to a fixed temperature for 2 h at each level. Within every 2 h sequence, we switched between the six cylinders which were placed horizontally on

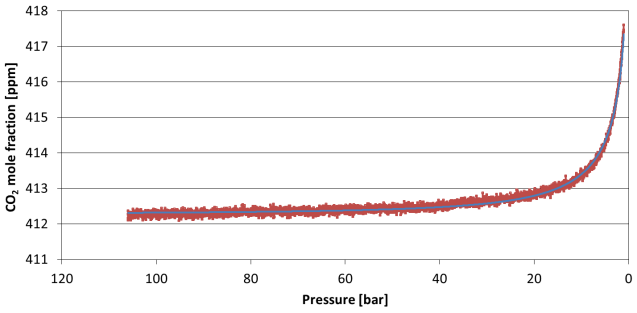

Figure 2. Emptying experiment within 14 h: CO_2 mole fraction of a steel cylinder vs. its pressure is shown in red (only every 100 point of 0.1 s resolution data is shown). The Langmuir monomolecular layer desorption model is shown in blue ($CO_{2,\,ad} = 0.41$ ppm, $K = 0.0436\,\mathrm{bar}^{-1}$).

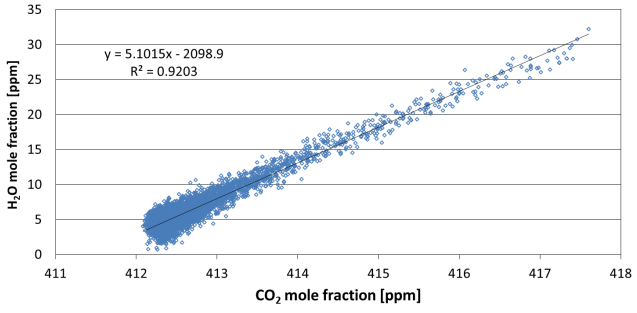

Figure 3. Emptying experiment within 14 h: H_2O even shows a 5-times stronger desorption effect documented by the linear correlation with the CO_2 mole fraction.

a wooden tray (Table 1), and an additional reference cylinder (CA03901) outside the climate chamber, using a 10-port VICI AG valve (type: EMT2CSD12MWE). Due to a leak, cylinder LK548528 had to be exchanged for cylinder LK535353 during the experiment. Unfortunately, the electronics of the VICI valve were malfunctioning after the first night (remained in the same position) and therefore we had to replace it. This sequence was neglected in the evaluation. The experiment was extended in order to obtain two full temperature cycles for data evaluation. The temperature in the climate chamber was measured directly on the cylinders using 80PK-1-type sensors with a range of −40 to +260 °C and was logged by a GMH3250 unit from Greisinger. The pressure transducers used were PTU-S-AC160-31AC for high pressures and PTU-S-AC6-31AC for low pressures, from Swagelok. Measurements were displayed by a homemade LCD device and logged by a Labjack U12 from Meilhaus Electronic GmbH.

Both cavity ring-down spectroscopy instruments are frequently calibrated with known standard gas admissions, i.e. in the case of experiment 1 before and after the experiment, and in the case of experiment 2, during the complete experiment; though the repeatability and drift rates are of more importance for these experiments that are designed to be short-term measurements. The repeatability can be accessed by the short-term measurement variability and corresponds to < 0.01 ppm (averaged over 5 min), whereas the drift rate was estimated from the standard cylinder CA03901 to be 0.0041 ppm day^{-1} (see also Sect. 3).

3 Results

Figure 2 displays the CO_2 mole fraction change for experiment 1 (emptying gas cylinders) for a steel cylinder. A significant CO_2 and H_2O (Fig. 3) mole fraction increase of 6 ppm (30 ppm for H_2O) is observed towards lower cylinder pressure in contrast to CH_4 which does not exhibit any change (not shown). One could argue, as detailed in Langenfelds et al. (2005), that ordinary diffusion is at play. Diffusion coefficients for CO_2 in air have been known for a long time (Kestin et al., 1984; Marrero and Mason, 1972; 1973). However, if one calculates the diffusion length, i.e. twice the square root of the product of the diffusion coefficient ($\approx 0.16\,\mathrm{cm}^2\,\mathrm{s}^{-1}$ for 20 °C and 1 bar (Massman, 1998)) and time (60 s), of CO_2 diffusion in air in a cylinder at high pressure (100 bar) corresponding to 6 mm and compares it to the radius of the gas volume at high pressure ($5\,\mathrm{L\,min}^{-1}$) that is decanted from the cylinder during our experiment 1, i.e. 27.7 mm, it has to be strongly questioned whether ordinary diffusion is responsible for the observed CO_2 increase. It is worthwhile mentioning that a comparison of the diffusion length with the radius of cylinders (100 mm) used for our experiments requires a diffusion time of 4 or 5 h, i.e. correspondent observation time is needed. Similar arguments can be used to exclude ordinary diffusion on the low pressure side, though with slightly lower confidence since the diffusion length is only half of the decanting volume. Furthermore, the diffusion fractionation should decrease with increasing gas flow, just opposite to what has been observed in Langenfelds et al. (2005), thermal diffusion induced by the Joule–Thomson cooling effect might only play a role for the low-flow decanting experiment, as shown below. Therefore, we follow the adsorption theory. According to Eq. (2), the initial CO_2 mole fraction ($CO_{2,\,\mathrm{initial}}$) can be calculated from the measured mole fraction ($CO_{2,\,\mathrm{meas}}$) through the following formula (see Appendix):

$$CO_{2,\,\mathrm{meas}} = CO_{2,\,\mathrm{ad}} \cdot \left(\frac{K \cdot (P - P_0)}{1 + K \cdot P} + (1 + K \cdot P_0) \cdot \ln\left(\frac{P_0 \cdot (1 + K \cdot P)}{P \cdot (1 + K \cdot P_0)} \right) - 1 \right) + CO_{2,\,\mathrm{initial}}, \quad (5)$$

where $CO_{2,\,\mathrm{ad}}$ corresponds to the adsorbed CO_2 molecules on the wall, expressed as CO_2 mole fraction multiplied by the occupied adsorption sites at pressure P_0. $CO_{2,\,\mathrm{ad}}$ and K can be determined experimentally from a fit of the measured CO_2 mole fraction. Note that K is temperature-dependent on the form as given in Eq. (5). For $P = P_0$, the measured CO_2 mole

fraction corresponds to the initial CO_2 mole fraction minus the adsorbed CO_2 amount. In our experiment this results in an adsorbed $CO_{2,\,ad}$ mole fraction of 0.41 ppm, corresponding to about 2.15 mL STP (standard temperature and pressure) ($P_0 = 105$ bar) or 96 micromoles of CO_2 or 5.8×10^{19} CO_2 molecules and 0.0436 bar^{-1} for K by minimization of the squared differences of Eq. (5) to the measured values. These values can be compared with a monomolecular layer of CO_2 molecules on the inner cylinder wall area. Our steel cylinders have an outer diameter of 0.24 m, an inner diameter of 0.2 m, and a length of 1.5 m. Therefore, the inner area corresponds roughly to 1 m^2, which is about 5 times lower than a monolayer of the adsorbed CO_2 molecules, corresponding to 5.25 m^2 when assuming a molecule diameter of 3.4 Å. It is interesting to note that the adsorbed water amount is about 5 times bigger (< 2.5 ppm) as shown by an equal pressure behaviour of desorption (Fig. 3) than for CO_2 (0.41 ppm). Considering the smaller molecule size for water would correspond to an even higher ratio to a monomolecular layer. The observed pressure dependence of both mole fractions shows only slightly increasing values in the range of 100 to 50 bar, contrasting the nature of a multiple layer adsorption isotherm (Brunauer et al., 1938). Hence, it seems plausible to question the validity of our assumption that the exposed adsorption surface corresponds to the geometric surface. Due to surface roughness, the adsorption surface might be significantly larger than the geometric measure. This is known in literature as rugosity. Values may range from 1 to more than 10 in the case of a sponge. For metals, surface roughness is more often expressed as Ra; i.e. the arithmetic mean of the surface height changes. These considerations justify using the Langmuir model.

Similar considerations can be made for the aluminium cylinder which results in empirically derived values of 0.047 ppm for $CO_{2,\,ad}$ and 0.001 bar^{-1} for K (Fig. 4). The effect of adsorption is significantly less on aluminium than on the steel surface; only about 35 % of the adsorption sites are occupied. This further supports our approach to use the Langmuir model for a monomolecular layer in contrast to a multi-layer coverage.

It was also tested whether the decanting rate has an influence, by performing tests with 5 and 0.25 L min^{-1}. The results are displayed in Fig. 4 and show similar increases towards lower pressures but there are obvious trends superimposed that cannot be explained by the adsorption theory. In particular the slightly decreasing mole fractions in the low-flow (0.25 L min^{-1}, Fig. 4, lower panel) decanting experiment on the aluminium cylinder is most probably a result of the Joule–Thomson effect; though instrumental drifts may play a role. However, our observation of drift rates under laboratory conditions using the instruments does not strongly support this. The Joule–Thomson effect leads to a significant temperature decrease of the gas and its surroundings at the regulator where the pressure decreases suddenly from high to ambient pressure (60 to 1 bar). The temperature decrease

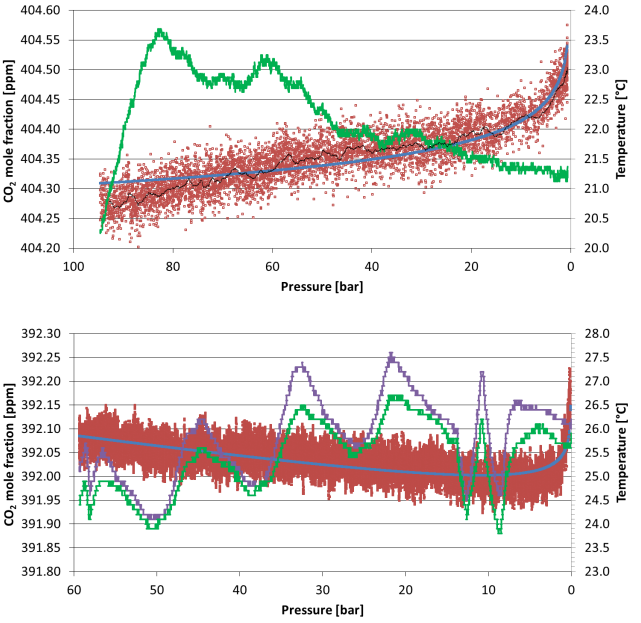

Figure 4. Fast- and slow-emptying experiment within 8 h (upper panel) and 120 h (lower panel), respectively: CO_2 mole fraction of an aluminium cylinder vs. its pressure in red (5 s resolution). The Langmuir monomolecular layer desorption model is shown in blue ($CO_{2,\,ad} = 0.047$ ppm, $K = 0.001$ bar^{-1}) for a decanting rate of 5 L min^{-1} in the upper panel and for 0.25 L min^{-1} in the lower panel ($CO_{2,\,ad} = 0.028$ ppm, $K = 0.001$ bar^{-1}). Temperature evolution corresponding to the pressure evolution is displayed for the aluminium cylinder (green line) and for the pressure regulator (in violet). Note that the decreasing trend can be explained by the Joule-Thompson cooling effect and has nothing to do with the adsorption theory. The desorption energies could not be determined with confidence during these decanting experiments.

can be estimated using the Joule–Thomson coefficient for air, i.e. +0.27 K bar^{-1}. For 100 bar pressure change, a temperature decrease of 27 K is estimated. The gas exposed to this temperature gradient suffers from thermal diffusion as the heavier gas constituents tend to move to the colder end and hence are enriched in the gas measured by the detector. However, the regulator temperature decrease by the gas cooling effect is partly compensated by the heat exchange with the surroundings. We used a symmetrically built two-stage Tescom regulator; therefore two-step cooling was induced. However, only the first cooling stage is important because this connects to the large gas volume in the cylinder, whereas from there on, fractionation cannot develop under quantitative transport of the gas into the analyser. It is difficult to determine the temperature distribution at the location where thermal fractionation due to the Joule–Thomson effect occurs. What we observe is exactly the opposite to our expectations, i.e. a CO_2 decrease pointing to a warmer temperature at the inter-stage compared to the high-pressure side. This requires further dedicated experiments.

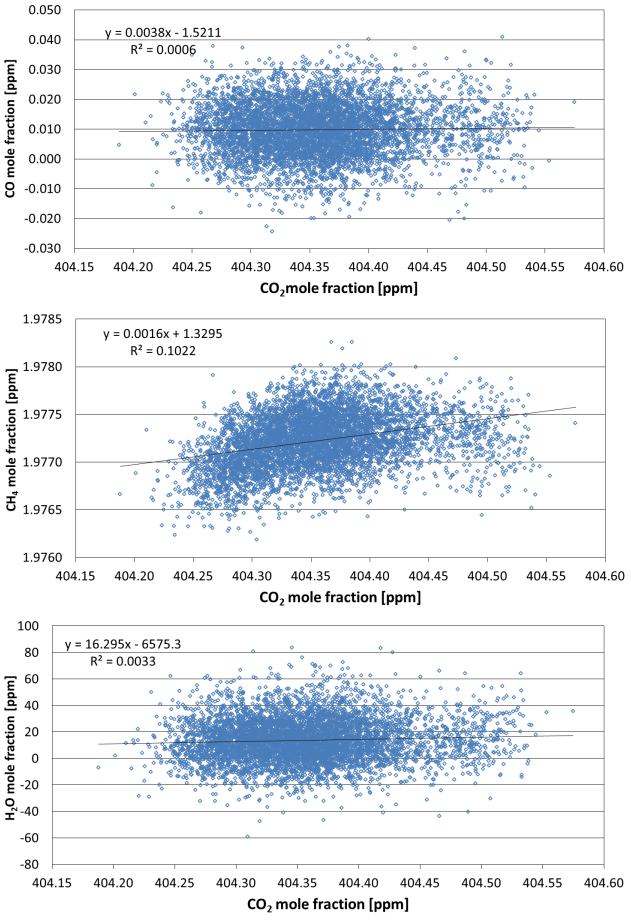

Figure 5. Decanting experiment within 8 h: no effect of CO and H_2O can be detected given the limitations of the analyser's signal-to-noise ratio at that level on the aluminium cylinder compared to the CO_2 mole fraction.

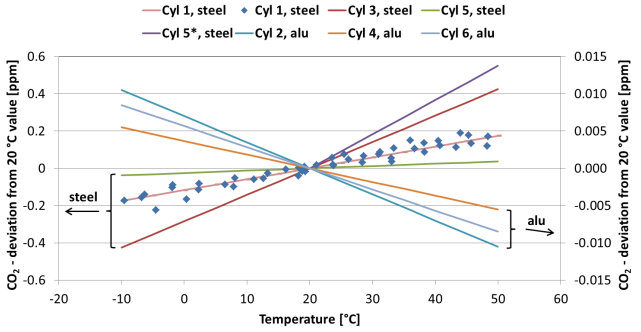

Figure 6. Temperature dependence for the CO_2 mole fraction deviations from their corresponding value at 20 °C (T_0) for the steel cylinders 1, 3, 5, 5* (increasing values, left y axis), as well as for aluminium cylinders 2, 4, 6 (decreasing values, right y axis). The y axes are different by a factor of 40. For clarity, measurements are only given for cylinder 1 (measurements for cylinder 2 are displayed in Fig. 8), together with its linear correlation line, whereas for the other cylinders, only linear correlations lines are given. The temperature dependencies vary between 0.0014 and 0.0184 ppm °C^{-1} for steel and −0.0002 and −0.0003 ppm °C^{-1} for aluminium cylinders.

Unlike the steel cylinder, the aluminium cylinder did not show any desorption effects for H_2O and CO, and it showed a hardly visible effect for CH_4, as displayed in Fig. 5. However, it has to be stressed that the H_2O and CO mole fractions were very low and further experiments should be done in particular for CO, including steel and aluminium cylinders.

The second experiment conducted in a climate chamber followed expectations in that the temperature dependence of CO_2 adsorption is considerable for steel surfaces but again significantly smaller for aluminium (Fig. 6). For the latter case it even changed sign to a slightly negative correlation with temperature, though this is statistically less robust than for steel. The temperature dependencies vary between 0.0014 to 0.0184 ppm °C^{-1} for steel and −0.0002 to −0.0003 ppm °C^{-1} for aluminium cylinders. The different sign of the dependencies for steel and aluminium cylinders is a first hint that these dependencies do not originate from instrument drift. This is supported by the measurements of cylinder CA03901, which acted as a reference that was not exposed to the temperature variations but was placed just beside the instrument in an anteroom. These measurements done throughout the experiment showed rather constant values with a standard deviation of 0.009 ppm on 5 min averages. There is only a small trend of +0.0041 ppm day^{-1} (not corrected in displays). Excluding the trend, the standard deviation reduces to 0.006 ppm. Furthermore, even with this small constant drift of the analyser, only the scatter of the data, but not the temperature dependence itself, would be affected. Actually, large instrument drifts could potentially be estimated from the scatter of the data. Therefore, the temperature dependencies seen for steel and aluminium cylinders are most certainly not due to drifts of the analyser. The pressure drop for gas consumption throughout this experiment was in the order of 14 and 24 bar, with initial pressures around 150 and 120 bar for the steel and aluminium cylinders, respectively (Table 1). The induced desorption changes are moderate and amount to about 0.01 ppm for both steel and aluminium cylinders according to Eq. (6). Also, the temperature-induced pressure changes amounting to about 30 bar (150 bar × $\Delta T/T$) are only twice as large. The relative influence on the temperature dependency observed for steel cylinders is expected to be minor. For the aluminium cylinders though, these influences are most probably the reason for the observed reversed temperature behaviour. Furthermore, we investigated whether the sealing material in use at the cylinder valve as well as at the connection to the pressure regulator (PEEK, PA) has an influence on our findings. An aluminium cylinder, not listed in Table 2, equipped with a VTI K44-8 (PEEK as spindle-sealing material) and with PA sealing at the regulator connection (G 5/8″ RH female thread), as used for the steel cylinders, showed similar

Table 2. Temperature dependencies of gas adsorption on steel and aluminium surfaces for CO_2 and H_2O applying a temperature range from −10 to +50 °C. NA when $r^2 < 0.02$. Temperature dependencies for CO and CH_4 could not be detected within experimental uncertainties.

Cylinder	CO_2 (ppm °C^{-1})	H_2O (ppm °C^{-1})	surface type
1: LK502291	0.0061	NA	steel
2: CB09790	−0.0003	NA	aluminium
3: LK548602	0.0141	NA	steel
4: CB09877	−0.0003	NA	aluminium
5: LK548528	0.0184	0.113	steel
5[a]: LK535353	0.0014	0.00003	steel
6: CB09786	−0.0003	NA	aluminium

[a] Due to a leak, cylinder LK548528 had to be exchanged for cylinder LK535353 during the experiment.

behaviour in an independent temperature sensitivity test to the aluminium cylinders used in this study, equipped with Rotarex D 202 valves (PA as spindle-sealing material) with gold rings as sealing material at the CGA 590 connections. All other measured gas species, i.e. CO, CH_4, and H_2O showed no temperature dependence as documented in Table 2, except for H_2O of the steel cylinder LK548528 that had to be replaced due to a leak. It is surprising that the leak obviously had no or at least not a strong effect on the derived thermal dependence, though the value for CO_2 is the highest observed. A reason for this behaviour might be that there is no fractionation associated with the leak (less plausible) or it remains constant and led only to a common shift of the mole fraction values but would not alter the temperature dependence.

According to Eq. (3), the coverage of the adsorption sites is temperature-dependent. The desorption and adsorption rates depend on whether we increase or decrease the temperature from a mean value. During the temperature increase (decrease) the adsorption rate will be lower (higher) than the desorption rate; and therefore the coverage of adsorption sites decreases (increases), while the gas mole fraction increases (decreases). A derivation of this temperature dependence is given in the Appendix that leads to Eq. (6):

$$R \cdot \ln\left(1 - \frac{\mathrm{CO_2}(T_0, T) - \mathrm{CO_2}(T_0)}{\mathrm{CO_{2,\,ad}}}\right) = E \cdot \left(\frac{1}{T} - \frac{1}{T_0}\right) - R \cdot \ln\left(\frac{\frac{T_0}{T} + P_0 \cdot K(T_0) \cdot e^{\frac{E}{R} \cdot \left(\frac{1}{T} - \frac{1}{T_0}\right)}}{1 + P_0 \cdot K(T_0)}\right). \quad (6)$$

Hence, during a temperature increase or decrease, we will determine the desorption energy, $E = E(\Theta)$, of the process when plotting the logarithm of 1 minus the temperature-scaled relative CO_2 mole fraction changes ($CO_2(T) - CO_2(T_0)$) to the adsorbed CO_2 vs. the difference of inverse temperatures. For steel cylinder 1, the values are plotted

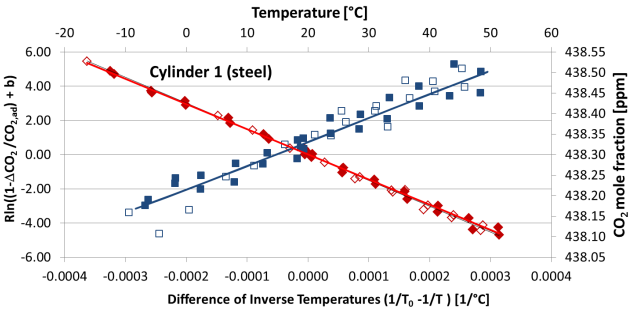

Figure 7. Dependence of scaled CO_2 mole fraction difference plus offset b on the difference of inverse temperature for the steel cylinder 1 according to Eq. (6). Open red symbols correspond to decreasing temperature; and filled red symbols correspond to increasing temperature shown in Fig. 1. The correlation is excellent ($r^2 = 1$), therefore the slopes correspond to the negative desorption energy (Eq. 6) as we have changed the x axis with a minus sign due to visibility reasons. The desorption energies do slightly differ from 14.74 to 15.10 kJ mol^{-1} for increasing and decreasing temperature, respectively, with a mean of 14.88 kJ mol^{-1} for the overall correlation using a $CO_{2,\,ad}$ value of 1.2 ppm and 0.0168 bar^{-1} for K_0. Open and filled blue symbols correspond to the CO_2 mole fractions vs. temperature, whereas the blue line corresponds to the estimated CO_2 mole fractions according to Eq. (A25).

in Fig. 7. From this graph or through Eq. (6), we now can estimate $CO_{2,\,ad}$, $K(T_0)$, and E by minimizing the squared differences of using Eq. (6) iteratively with initial values obtained from experiment 1 for steel and aluminium cylinders, respectively. The slopes corresponding to the desorption energies for positive and negative temperature gradients do only slightly differ and vary between 14.74 ± 0.17 and 15.10 ± 0.25 kJ mol^{-1}, with an average value of 14.88 ± 0.14 kJ mol^{-1} for all measurements using a value of 1.2 ppm for $CO_{2,\,ad}$ and 0.0168 bar^{-1} for K_0. For the aluminium cylinders it looks very different with very low and even reversed temperature dependencies, which indicates lower desorption based on the dependence given in Eq. (6). This equation shows a sign change for desorption energies around 2.43 kJ mol^{-1} when setting T_0 to 20 °C. This sign change moves towards zero when T_0 approaches absolute zero (see Appendix, Eqs. A25–A27). Indeed, the optimized desorption energy (1.58 kJ mol) for aluminium cylinder 2 is below this threshold of 2.43 kJ mol^{-1} using a value of 0.45 ppm for $CO_{2,\,ad}$ and 0.001 bar^{-1} for K_0. The significantly lower correlation ($r^2 < 0.75$) than for the steel cylinder (Fig. 7) can only partly be explained by the very small effects observed for the aluminium cylinders ($\Delta CO_2 < 0.04$ ppm) since the measurement repeatability is below 0.006 ppm as documented by the reference cylinder (CA03901). This calls for additional influences. The fact that there are small offsets observed for the CO_2 mole fraction for positive and negative temperature gradients (dotted red lines in Fig. 8) may indicate a temperature-driven influence. A small contribution of

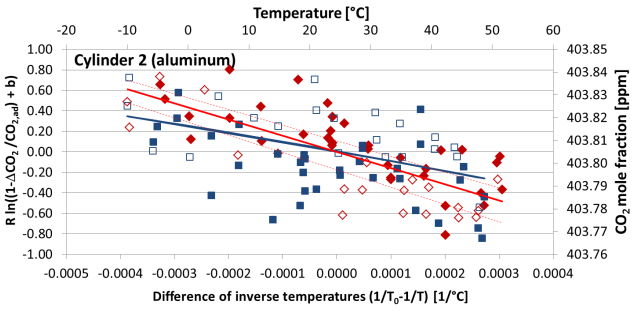

Figure 8. Dependence of scaled CO_2 mole fraction difference plus offset b on the difference of inverse temperature for the aluminium cylinder 2 according to Eq. (6). Open red symbols correspond to decreasing and filled red symbols to increasing temperature in Fig. 1 together with their corresponding correlation lines (dotted red lines). The red line corresponds to all values. The slopes correspond to the negative desorption energy (Eq. 6) as we have changed the x axis as in Fig. 7. The correlation is rather weak ($r^2 = 0.6$). Part of the variability might be due to temperature-induced effects that are independent of adsorption/desorption phenomena. Hence care has to be taken with desorption energies of 1.53 kJ mol^{-1} increasing to 1.68 kJ mol^{-1} for decreasing temperature with a mean of 1.58 kJ mol^{-1}. Open and filled blue symbols correspond to the CO_2 mole fractions vs. temperature, whereas the blue line corresponds to the estimated CO_2 mole fractions according to Eq. (A25).

thermal diffusion to the measured CO_2 mole fraction (Keeling et al., 2007) as discussed above can therefore not be excluded and requires further attention, e.g. regarding temperature distribution on regulators. Therefore the determination of the desorption energy for aluminium cylinders is difficult due to the very small, hardly measurable CO_2 change. Hence care should be taken with those values that are lower than for steel cylinders.

4 Conclusion

The experiments performed clearly demonstrate that the aluminium cylinders are significantly more robust against adsorption/desorption processes for CO_2, CO, CH_4, and H_2O than steel cylinders. The CO_2 desorption rate behaviour follows a pressure-driven monomolecular layer desorption as described by the Langmuir equation nicely and is about 10 times larger for steel than for aluminium surfaces. Also, the adsorbed amount is about 10 times higher for steel (0.41 ppm) than for aluminium (0.028 and 0.047 ppm). The mole fractions close to atmospheric pressure are strongly influenced and reach values of about 100 times larger than the World Meteorological Organization (WMO) target value of 0.1 ppm for steel and values still significantly above that for aluminium. Therefore, special attention has to be paid to which end pressure the cylinders should be used for calibration purposes. The community is generally aware of this influence that has been investigated by Chen et al. (2013), but it has not yet been properly quantified. It is noteworthy that desorption starts already close to 100 bar (1450 per square inch gauge). At 30 bar it can already reach 0.5 ppm for steel cylinders. The WMO target value of 0.1 ppm might already be reached at 60 bar compared to the value at 100 bar.

The temperature dependence that was observed for three steel and aluminium cylinders ranged from 0.0014 to 0.0184 ppm °C^{-1} and from −0.0002 to −0.0003 ppm °C^{-1}, respectively. This might have an influence on the precision when facing large temperature fluctuations in the laboratories or when measuring in the field with large ambient temperature variations – but only for steel and not for aluminium cylinders. A robust estimate of the desorption energy was possible only for steel (14.9 kJ mol^{-1}) but not for aluminium, due to the low temperature dependence and temperature range investigated. The determined energy value underpins that the observed adsorption mechanism is physisorption only.

The two experiments are qualitatively in agreement in the present study; however, they were carried out on different cylinders. Similar experiments are required using exactly the same cylinders, i.e. first determining the temperature dependence following by the decanting experiment. This would allow the consistency of the estimated parameters $CO_{2,\,ad}$, K_0, and E to be checked.

The recommendation for high-precision trace gas determination is to use aluminium cylinders and to minimize temperature fluctuations in order to limit desorption and thermal diffusion effects, and that the usage should be restricted to pressure above 30 bar to remain within the WMO target.

Appendix A: Derivation of Eqs. (5) and (6)

During experiment 1, gas is decanted from a cylinder with a fixed volume, V, and at a constant temperature, T, after air with an initial CO_2 mole fraction, $CO_{2,\,\mathrm{initial}}$, i.e. $n_{CO_2,\,\mathrm{initial}}/n_{\mathrm{air}}$, is compressed into a cylinder to a pressure, P_0. After reaching adsorption equilibrium, the CO_2 mole fraction in the cylinder is reduced by $CO_{2,\,\mathrm{ad}}$. The CO_2 amount, n_{CO_2}, in the gas phase of the cylinder at any pressure, P, is expressed using the ideal gas law by

$$n_{CO_2} = n_{\mathrm{air}} \cdot CO_2 = \frac{P \cdot V}{R \cdot T} \cdot CO_2, \tag{A1}$$

where R is the ideal gas constant and CO_2 is the mole fraction of CO_2. Assuming that CO_2 adsorption/desorption follows Eqs. (2) and (3), the Langmuir's adsorption isotherm, the amount adsorbed at pressure P, n_{ad}, is expressed in relation to the inversely scaled adsorbed amount at pressure P_0, a, according to

$$n_{\mathrm{ad}}(P) = a \cdot \frac{K P}{1 + K P} \tag{A2}$$

$$n_{\mathrm{ad}}(P_0) = a \cdot \frac{K P_0}{1 + K P_0} = \frac{P_0 \cdot V}{R \cdot T} \cdot CO_{2,\,\mathrm{ad}}. \tag{A3}$$

This results in

$$a = \frac{P_0 \cdot V}{R \cdot T} \cdot CO_{2,\,\mathrm{ad}} \cdot \frac{1 + K P_0}{K P_0} = \frac{1 + K P_0}{K} \cdot \frac{V}{R \cdot T} \cdot CO_{2,\,\mathrm{ad}}, \tag{A4}$$

which results in

$$n_{\mathrm{ad}}(P) = (1 + K P_0) \cdot \frac{V}{R \cdot T} \cdot CO_{2,\,\mathrm{ad}} \cdot \frac{P}{1 + K P}, \tag{A5}$$

where K represents the equilibrium constant at constant temperature, T ($K = k/k_{-1}$). In the case of experiment 2, the temperature dependence of K needs to be taken into account.

Thus the change in the CO_2 amount in the gas phase of the cylinder according to pressure change is expressed by the following differential equation:

$$\frac{\mathrm{d}n_{CO_2}}{\mathrm{d}P} = \frac{n_{CO_2}}{P} - \frac{\mathrm{d}n_{\mathrm{ad}}}{\mathrm{d}P}. \tag{A6}$$

The first term on the right-hand side corresponds to the change in the CO_2 amount due to the gas pressure change during gas decanting. The second term describes the effect of the CO_2 desorption from the inner cylinder walls that can be derived from the derivative of Eq. (A5):

$$\frac{\mathrm{d}n_{CO_2}}{\mathrm{d}P} = \frac{n_{CO_2}}{P} - \frac{(1 + K P_0) \cdot \frac{V}{R \cdot T} \cdot CO_{2,\,\mathrm{ad}}}{(1 + K P)^2}. \tag{A7}$$

Solving the differential Eq. (A6) yields

$$n_{CO_2} = c \cdot P - (1 + K P_0) \cdot \frac{V}{R \cdot T} \cdot CO_{2,\,\mathrm{ad}} \cdot P \cdot \left(\frac{1}{1 + K P} + \ln(K P) - \ln(1 + K P) \right). \tag{A8}$$

With

$$n_{CO_2}(P_0) = P_0 \cdot \frac{V}{R \cdot T} \cdot \left(CO_{2,\,\mathrm{initial}} - CO_{2,\,\mathrm{ad}} \right),$$

it follows

$$c = \frac{V}{R \cdot T} \cdot CO_{2,\,\mathrm{initial}} + (1 + K P_0) \cdot \frac{V}{R \cdot T} \cdot CO_{2,\,\mathrm{ad}} \cdot \ln\left(\frac{K P_0}{1 + K P_0} \right),$$

and therefore

$$n_{CO_2} = \frac{P \cdot V}{R \cdot T} \left(CO_{2,\,\mathrm{ad}} \cdot \left(\frac{K (P - P_0)}{1 + K P} + (1 + K P_0) \cdot \ln\left(\frac{P_0 \cdot (1 + K P)}{P \cdot (1 + K P_0)} \right) - 1 \right) + CO_{2,\,\mathrm{initial}} \right). \tag{A9}$$

Therefore, the measured CO_2 mole fraction of the cylinder according to Eq. (A1), can be expressed as

$$CO_{2,\,\mathrm{meas}} = CO_{2,\,\mathrm{ad}} \cdot \left(\frac{K (P - P_0)}{1 + K P} + (1 + K P_0) \cdot \ln\left(\frac{P_0 \cdot (1 + K P)}{P \cdot (1 + K P_0)} \right) - 1 \right) + CO_{2,\,\mathrm{initial}}, \tag{A10}$$

which corresponds to Eq. (5) in the main text.

Derivation of Eq. (6)

During experiment 2, cylinders are exposed to temperature changes and only a small amount of gas is decanted from a cylinder for analysis. Therefore, we assume that the changes in CO_2 mole fraction in the gas phase are only due to adsorption changes associated with direct temperature and pressure changes that are induced by it.

$$\frac{\mathrm{d}n_{CO_2}}{\mathrm{d}T} = -\frac{\mathrm{d}n_{\mathrm{ad}}}{\mathrm{d}T} \tag{A11}$$

$$n_{CO_2}(T) = \mathrm{C} - n_{\mathrm{ad}}(T) \tag{A12}$$

$$n_{CO_2}(T_0) = C - n_{\mathrm{ad}}(T_0) = n_{\mathrm{initial}} - n_{\mathrm{ad}}(T_0) \tag{A13}$$

$$n_{CO_2}(T) - n_{CO_2}(T_0) = n_{\mathrm{ad}}(T_0) - n_{\mathrm{ad}}(T) \tag{A14}$$

According to Eq. (4) in the main text the temperature dependence of K can be written as

$$K(T) = \frac{k}{k_{-1}} = K(T_0) \cdot e^{\frac{E}{R} \cdot \left(\frac{1}{T} - \frac{1}{T_0} \right)}. \tag{A15}$$

We can generalize Eq. (A2) with Eq. (A15) to Eq. (A16) and Eq. (A17):

$$n_{\mathrm{ad}}(PT) = a \cdot \frac{P \cdot K(T_0) \cdot e^{\frac{E}{R} \cdot \left(\frac{1}{T} - \frac{1}{T_0} \right)}}{1 + P \cdot K(T_0) \cdot e^{\frac{E}{R} \cdot \left(\frac{1}{T} - \frac{1}{T_0} \right)}} \tag{A16}$$

$$n_{\mathrm{ad}}(P_0, T_0) = a \cdot \frac{1 + P_0 \cdot K(T_0)}{P_0 \cdot K(T_0)} = \frac{P_0 \cdot V}{R \cdot T_0} \cdot CO_{2,\,\mathrm{ad}}. \tag{A17}$$

This results in

$$a = \frac{P_0 \cdot V}{R \cdot T_0} \cdot CO_{2,\,\mathrm{ad}} \cdot \frac{1 + P_0 \cdot K(T_0)}{P_0 \cdot K(T_0)}, \tag{A18}$$

which results in

$$n_{\mathrm{ad}}(P,\mathrm{T}) = \frac{P_0 \cdot V}{R \cdot T_0} \cdot \mathrm{CO}_{2,\,\mathrm{ad}} \cdot \frac{1 + P_0 \cdot K(T_0)}{P_0 \cdot K(T_0)} \cdot \frac{P \cdot K(T_0) \cdot e^{\frac{E}{R} \cdot \left(\frac{1}{T} - \frac{1}{T_0}\right)}}{1 + P \cdot K(T_0) \cdot e^{\frac{E}{R} \cdot \left(\frac{1}{T} - \frac{1}{T_0}\right)}} \quad \text{(A19)}$$

$$\mathrm{CO}_{2,\,\mathrm{ad}}(P,\,T) = \frac{R \cdot T}{\mathrm{P} \cdot V} \cdot n_{\mathrm{ad}}(P,\,T) \quad \text{(A20)}$$

$$\mathrm{CO}_{2,\,\mathrm{ad}}(P,\,T) = \frac{R \cdot T}{P \cdot V} \cdot \frac{P_0 \cdot V}{R \cdot T_0} \cdot \mathrm{CO}_{2,\,\mathrm{ad}} \cdot \frac{1 + P_0 \cdot K(T_0)}{P_0 \cdot K(T_0)} \cdot \frac{P \cdot K(T_0) \cdot e^{\frac{E}{R} \cdot \left(\frac{1}{T} - \frac{1}{T_0}\right)}}{1 + P \cdot K(T_0) \cdot e^{\frac{E}{R} \cdot \left(\frac{1}{T} - \frac{1}{T_0}\right)}}. \quad \text{(A21)}$$

Since the amount of air does not change during experiment 2, we follow

$$\frac{R \cdot T}{P \cdot V} \cdot \frac{P_0 \cdot V}{R \cdot T_0} = \frac{P_0}{P} \cdot \frac{T}{T_0} = 1 \quad \text{(A22)}$$

$$\mathrm{CO}_{2,\,\mathrm{ad}}(P,\,T) = \mathrm{CO}_{2,\,\mathrm{ad}} \cdot \frac{1 + P_0 \cdot K(T_0)}{P_0 \cdot K(T_0)} \cdot \frac{P \cdot K(T_0) \cdot e^{\frac{E}{R} \cdot \left(\frac{1}{T} - \frac{1}{T_0}\right)}}{1 + P \cdot K(T_0) \cdot e^{\frac{E}{R} \cdot \left(\frac{1}{T} - \frac{1}{T_0}\right)}}. \quad \text{(A23)}$$

With Eq. (A23), Eq. (A14) can be rearranged to

$$\mathrm{CO}_2(T_0,\,T) - \mathrm{CO}_2(T_0) = \mathrm{CO}_{2,\,\mathrm{ad}} - \mathrm{CO}_{2,\,\mathrm{ad}} \cdot \frac{1 + P_0 \cdot K(T_0)}{P_0 \cdot K(T_0)} \cdot \frac{P \cdot K(T_0) \cdot e^{\frac{E}{R} \cdot \left(\frac{1}{T} - \frac{1}{T_0}\right)}}{1 + P \cdot K(T_0) \cdot e^{\frac{E}{R} \cdot \left(\frac{1}{T} - \frac{1}{T_0}\right)}} \quad \text{(A24)}$$

$$\mathrm{CO}_2(T_0,\,T) - \mathrm{CO}_2(T_0) = \mathrm{CO}_{2,\,\mathrm{ad}} \cdot \left(1 - \frac{1 + P_0 \cdot K(T_0)}{P_0 \cdot K(T_0)} \cdot \frac{P \cdot K(T_0) \cdot e^{\frac{E}{R} \cdot \left(\frac{1}{T} - \frac{1}{T_0}\right)}}{1 + P \cdot K(T_0) \cdot e^{\frac{E}{R} \cdot \left(\frac{1}{T} - \frac{1}{T_0}\right)}}\right). \quad \text{(A25)}$$

It is noteworthy that Eq. (A25) has a root at energies around 2430 J mol[1] for T_0 at 293.15 °C. A general dependence of $E_0(T, T_0)$ corresponds to

$$E_0(T,\,T_0) = \frac{R}{\left(\frac{1}{T} - \frac{1}{T_0}\right)} \cdot \ln\left(\frac{T_0}{T}\right) = \frac{R \cdot T \cdot T_0}{(T_0 - T)} \cdot \ln\left(\frac{T_0}{T}\right) \quad \text{(A26)}$$

above which Eq. (A25) is increasing and below which it is decreasing. E_0 approaches zero when T_0 is close to a temperature of absolute zero. This is important for the different adsorption/desorption behaviour on steel and aluminium cylinders (see main text).

$$R \cdot \ln\left(1 - \frac{\mathrm{CO}_2(T_0,\,T) - \mathrm{CO}_2(T_0)}{\mathrm{CO}_{2,\,\mathrm{ad}}}\right) = E \cdot \left(\frac{1}{T} - \frac{1}{T_0}\right) - R \cdot \ln\left(\frac{\frac{T_0}{T} + P_0 \cdot K(T_0) \cdot e^{\frac{E}{R} \cdot \left(\frac{1}{T} - \frac{1}{T_0}\right)}}{1 + P_0 \cdot K(T_0)}\right) \quad \text{(A27)}$$

This equation allows us to estimate $\mathrm{CO}_{2,\,\mathrm{ad}}$, $K(T_0)$, and E by minimizing the squared differences of using Eq. (A27) with initial values obtained from experiment 1 for steel and aluminium cylinders, respectively. This yields a $\mathrm{CO}_{2,\,\mathrm{ad}}$ of 1.2 ppm, $K(T_0)$ of 0.0168 bar^{-1}, and a desorption energy of $14\,882 \pm 176$ J mol^{-1} for cylinder 1 (steel, robust estimate). The estimates for aluminium cylinders are significantly less robust due to much smaller adsorption/desorption effects.

Acknowledgements. This is a contribution to the CarboCount CH Sinergia project financed by the Swiss National Science Foundation (CRSII2_136273). We thank Rüdiger Schanda for helping us with the measuring device. We are also grateful to the national and international intercomparison initiatives, such as Round Robins organized by WMO/IAEA, the Cucumber program organized by UEA, and others that were helpful in leading to these investigations. We are very grateful for the comments of three anonymous reviewers that significantly improved the ACPD manuscript and additionally to a reviewer of the primarily revised manuscript for ACP, furthermore for two additional reviewers of AMTD.

Edited by: T. von Clarmann

References

Bender, M. L., Tans, P. P., Ellis, J. T., Orchardo, J., and Habfast, K.: A high-precision isotope ratio mass-spectrometry method for measuring the O_2 N_2 ratio of air, Geochim. Cosmochim. Ac., 58, 4751–4758, 1994.

Berhanu, T. A., Satar, E., Schanda, R., Nyfeler, P., Moret, H., Brunner, D., Oney, B., and Leuenberger, M.: Measurements of greenhouse gases at Beromünster tall tower station in Switzerland, Atmos. Meas. Tech. Discuss., 8, 10793–10822, doi:10.5194/amtd-8-10793-2015, 2015.

Brunauer, S., Emmett, P. H., and Teller, E.: Adsorption of Gases in Multimolecular Layers, J. Am. Chem. Soc., 60, 309–319, 1938.

Chen, H.: Long-term stability of calibration gases in cylinders for CO_2, CH_4, CO, N_2O, and SF_6, in 17th WMO(IAEA meeting on Carbon Dioxide , other greenhouse gases and related measurement techniques (GGMT-2013), edited by: WMO/IAEA, Chinese Meterological Administration, Beijing, China, 2013.

Freundlich, H. M. F.: Über die Adsorption in Lösungen., Z. Phys. Chem., 57, 385–470, 1906.

Keeling, R. F., Manning, A. C., McEvoy, E. M., and Shertz, S. R.: Methods for measuring changes in atmospheric O_2 concentration and their application in southern hemisphere air, J. Geophys. Res.-Atmos., 103, 3381–3397, 1998.

Keeling, R. F., Manning, A. C., Paplawsky, W. J., and Cox, A. C.: On the long-term stability of reference gases for atmospheric O_2/N_2 and CO_2 measurements, Tellus B, 59, 3–14, 2007.

Kestin, J., Knierim, K., Mason, E. A., Najafi, B., Ro, S. T., and Waldman, M.: Equilibrium and transport-properties of the noble-gases and their mixtures at low-density, J. Phys. Chem. Ref. Data, 13, 229–303, 1984.

Langenfelds, R. L., van der Schoot, M. V., Francey, R. J., Steele, L. P., Schmidt, M., and Mukai, H.: Modification of air standard composition by diffusive and surface processes, J. Geophys. Res.-Atmos., 110, D13307, doi:10.1029/2004JD005482, 2005.

Langmuir, I.: The constitution and fundamental properties of solids and liquids, J. Am. Chem. Soc., 38, 2221–2295, 1916.

Langmuir, I.: The adsorption of gases on plane surfaces of glass, mica and platinum, J. Am. Chem. Soc., 40, 1361–1403, 1918.

Marrero, T. R. and Mason, E. A.: Gaseous Diffusion Coefficients, J. Phys. Chem. Ref. Data, 1, 3–118, 1972.

Marrero, T. R. and Mason, E. A.: Correlation and prediction of gaseous diffusion-coefficients, Aiche J., 19, 498–503, 1973.

Massman, W. J.: A review of the molecular diffusivities of H_2O, CO_2, CH_4, CO, O_3, SO_2, NH_3, N_2O, NO, and NO_2 in air, O_2 and N_2 near STP, Atmos. Environ., 32, 1111–1127, 1998.

Matsumoto, N., Watanabe, T., and Kato, K.: Effect of moisture adsorption/desorption on external cylinder surfaces: influence on gravimetric preparation of reference gas mixtures, Accredit. Qual. Assur., 10, 382–385, 2005.

Schibig, M. F., Steinbacher, M., Buchmann, B., van der Laan-Luijkx, I. T., van der Laan, S., Ranjan, S., and Leuenberger, M. C.: Comparison of continuous in situ CO_2 observations at Jungfraujoch using two different measurement techniques, Atmos. Meas. Tech., 8, 57–68, doi:10.5194/amt-8-57-2015, 2015.

Yokohata, A., Makide, Y., and Tominaga, T.: A new calibration method for the measurement of CCL4 concentration at 10-10 V/V level and the behavior of CCL4 in the atmosphere, B. Chem. Soc. JPN, 58, 1308–1314, 1985.